Theor Chem Acc (2012) 131:1240
DOI 10.1007/s00214-012-1240-9

REGULAR ARTICLE

Assessing the accuracy of a QM/MM//MD combined protocol to compute spectromagnetic properties of polyfunctional nitroxides in solution

Céline Houriez · Nicolas Ferré · Didier Siri · Paul Tordo · Michel Masella

Received: 24 April 2012 / Accepted: 25 April 2012 / Published online: 13 June 2012

Abstract In the field of spin trapping chemistry, we proposed a promising new theoretical QM/MM//MD combined protocol to assist the development of new nitrone-based spin traps (Houriez et al. in J Phys Chem B 114:11793–11803, 2010). In the present study, we test its accuracy and its transferability by investigating the spectromagnetic properties in water of DMPO–OH, the nitroxide spin adduct of the 5,5-dimethyl-1-pyrroline-*N*-oxide nitrone (DMPO) with the $OH^{\cdot}$ radical. Thanks to our theoretical method, we obtain quantitative estimates of the DMPO–OH hyperfine coupling constants (hcc's) in very good agreement with experiment. Moreover, our study reveals that the DMPO–OH hcc values are related to the main features of an equilibrium between two major conformations of the nitroxide five-membered ring. Together with our earlier results, the present study clearly establishes the reliability of our theoretical protocol to investigate in condensed phase the behavior of flexible and large nitroxides. Particularly, note that with our method, it is possible to point out clearly fundamental differences in spectromagnetic properties even for two molecules very similar in geometrical structure.

Keywords Spectromagnetic properties · Hyperfine coupling constants · Nitroxides · Liquid phase · QM/MM computations · Polarizable force field · Molecular dynamics

1 Introduction

A major challenge in the field of spin trapping is the development of theoretical protocols able to predict reliable electronic paramagnetic resonance (EPR) spectra for flexible molecules embedded in water or in heterogeneous chemical environments. Recently, we proposed such a protocol to compute hyperfine coupling constants (hcc's) of flexible nitroxides in water [1, 2]. It is based on combining nanosecond-scale classical molecular dynamics (MD) with large-scale QM/MM computations on small nitroxide/water clusters extracted along the MD trajectories. One originality of our protocol is the use of an ad hoc parameterized polarizable force field to generate the MD trajectories. We may note that applying a specially tailored classical force field has recently gained a renewed interest [3] as a good alternative to DFT-based computations [4–7].

Thanks to that protocol, we investigated previously the behavior in liquid water of the DMPO–OOH spin adduct resulting from the reaction of the 5,5-dimethyl-1-pyrroline-*N*-oxide (DMPO), a five-membered ring cyclic nitrone, with the $O_2^{-\cdot}$ superoxide radical [8] (see Fig. 1). We

Electronic supplementary material The online version of this article (doi:10.1007/s00214-012-1240-9) contains supplementary material, which is available to authorized users.

C. Houriez (✉)
Laboratoire Modélisation et Simulations Multi-Échelle,
Université Paris-Est Marne-la-Vallée,
77420 Champs-sur-Marne, France
e-mail: celine.houriez@univ-provence.fr

N. Ferré · D. Siri · P. Tordo
Université d'Aix-Marseille, Institut de Chimie Radicalaire,
Avenue Escadrille Normandie-Niemen,
13397 Marseille Cedex 20, France

M. Masella
Laboratoire de Chimie du Vivant, Service d'ingénierie
moléculaire des protéines, Institut de biologie et de technologies
de Saclay, Commissariat à l'énergie atomique, Centre de Saclay,
91191 Gif-sur-Yvette Cedex, France

evidenced that two main conformer families (or sites) of DMPO–OOH have to be observed in solution. They are characterized by the value of the ∠COOH dihedral angle and it exists within these sites a fast interconversion process between two major conformations of the nitroxide five-membered ring. Moreover, we showed that the nitroxide nitrogen and β and γ-hydrogen hcc's for both sites linearly depend on the ring conformation equilibrium ratio, explaining the noticeable asymmetry of the DMPO–OOH EPR spectrum [9]. Note that we showed a 1:1 ratio to provide hcc values for both sites agreeing within 0.5 Gauss with those extrapolated from recent deuterated experiments [10].

The DMPO nitrone may also react with the $OH^{\cdot}$ hydroxyl radical [9, 11], leading to the DMPO–OH spin adduct characterized by a simplier EPR spectrum, relative to DMPO–OOH (see Fig. 1). Moreover, the β-hydrogen hcc value of DMPO–OH differs significantly from its DMPO–OOH counterpart, up to 4 Gauss, and we may also note that no γ-hydrogen splitting is reported for DMPO–OH, whereas such a splitting plays a key role in the DMPO–OOH EPR spectrum asymmetry.

Theoretical computations on DMPO–OH are rather scarce [12–15], and the attempts to evaluate theoretically its hcc's in aqueous solution lead to values that do not agree with experiment [15]. Hence, our theoretical protocol is applied here to this problem, and our results allow one to assess the predictive ability of our method, notably in the particular case of molecules very close in structure but whose spectromagnetic properties differ strongly, like DMPO–OH and DMPO–OOH.

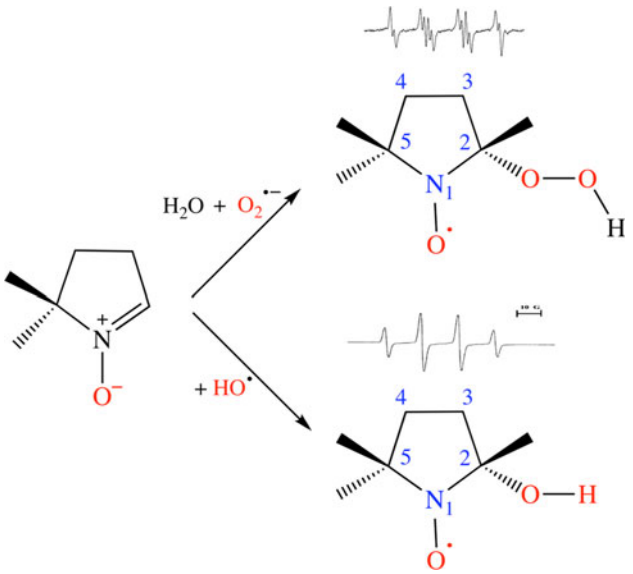

Fig. 1 Spin trapping of the $OH^{\cdot}$ hydroxyl and $O_2^{\cdot-}$ superoxide radicals by the DMPO nitrone, and the corresponding EPR spectra for the resulting adducts, namely DMPO–OOH (*above*) and DMPO–OH (*below*)

2 Computational details

We detail here two key points of our QM/MM//MD protocol, namely the polarizable force field parameters and the QM/MM coupling method. This protocol includes the generation of 8-ns-long trajectories of a nitroxide embedded in a large water box, using periodic boundary conditions and Ewald summation techniques. The details of our simulations may be found elsewhere [8].

2.1 Force field parameters and DMPO–OH five-membered ring flexibility

We use the TCPEp polarizable force field [16] based on a decomposition of the system potential energy into five terms corresponding to a repulsive, a classical charge–charge electrostatic, an intramolecular relaxation, a polarization and a specific hydrogen bond (HB) terms. A special stretch-torsion coupling term is added to the HB term to account for the anomeric effects affecting the CH_β and CO bonds in nitroxides [8]. To model the HB's occurring between the nitroxide hydroxyl moiety and the water molecules, we consider the HB term described in Ref. [16], whose parameters are assigned to reproduce the ab initio potential energy surface (PES) of methanol/$(water)_n$ aggregates ($n = 1$–3).

In line with our earlier studies [8, 17], we handle the nitrogen out-of-plane displacement by using a harmonic potential $U_{imp} = k_{imp}\theta^2$, where θ is the ∠ONCC improper dihedral angle. We assign k_{imp} together with the parameters of the torsional energy term corresponding to the dihedral angle $\phi = \angle H_\beta CNC$. This allows us to reproduce accurately the quantum PES as a function of (θ, ϕ) for the IPENO–OH model nitroxide (see Supporting Information for details).

We characterize the intrinsic flexibility of the DMPO–OH five-membered ring thanks to the ω phase of the ring deformation, as proposed by Cremer and Pople [18]. Whatever the ring conformation [envelope (E) or twist (T)], we denote by $^3T_4$ ($^4T_3$) a conformation in which the ring carbon 3 (4) is above the ring mean plane (see Fig. 1). We define for DMPO–OH eight force field parameter sets allowing us to generate trajectories corresponding to various $^3T_4/^4T_3$ equilibrium ratios in solution (from 1/99 to 97/3 %). Those sets, labeled T1–T8 like the corresponding trajectories in solution, differ only by the torsional parameters related to the ∠OCCC and $\angle H_\beta CCC$ ring dihedral angles. Concerning the energetic results for the $^3T_4$ and $^4T_3$ conformers of DMPO–OH in gas phase, if we

compare those derived from our force field approaches and those obtained from B3LYP and MP2 quantum computations, we note that the T4 parameter set provides the best agreement with quantum data. That force field predicts the $^3T_4/^4T_3$ equilibrium ratio for DMPO–OH in solution to be 34/66 %.

2.2 Quantum computations of average hcc's

For a monoradical, the a_X isotropic hcc (corresponding to the Fermi contact term) depends linearly on the ρ_s^X electronic spin density evaluated at the X nucleus

$$a_X = \frac{8\pi}{3} g_e \mu_e g_n^X \mu_n^X \rho_s^X \quad (1)$$

where g_n^X and μ_n^X are, respectively, the Landé g factor and the Bohr magneton of the nucleus, and g_e and μ_e correspond to the electron [19]. All quantum computations are performed using the Gaussian 03 package of programs [20], in which we incorporated locally the ESPF method [21] allowing one to account for the electrostatic potential generated by the solvent bulk on the extracted cluster nuclei. The instantaneous hcc's along the trajectories are computed using the cheap PBE0/6-31+G(d) level of theory, whose accuracy for our present purpose is equivalent within about 0.5 Gauss on average to the much more demanding CCSD/EPR-II level (see below).

The $\bar{a}_X$ hcc values of the solvated nitroxides are averaged on statistical ensembles including 2000 structures extracted each 1 ps along the trajectories. The sampling starts after an equilibration period of 6 ns and goes on during 2 ns. We check that a sampling interval of 1 ps leads to a set of temporally uncorrelated nitroxide/water structures by sampling each 5 fs two 50 ps trajectory segments of DMPO–OH in solution along which the ring conformation corresponds to a pure $^3T_4$ or $^4T_3$ one. The corresponding $C_{a_N}(t)$ and $C_{a_{H_\beta}}(t)$ autocorrelation functions were then computed: whatever the trajectory and the hcc, the serial correlation died usually after about 500 fs, insuring a 1 ps sampling interval to be well suited for the present purpose.

3 Results and discussion

Except for the hcc's (see above), all the statistical averages and distribution functions discussed in that section are computed along the last 6 ns segments of the 8 solvated trajectories. Several details concerning these results are provided as Supporting Information.

3.1 DMPO–OH conformations in solution

We compute the g_ω distribution functions corresponding to the ω phase characterizing the five-membered ring conformation along the trajectories: they all present two well-defined peaks at 85–95° and 255–275°, and a flat and almost null minimum at 180°. Hence, a $^3T_4/^4T_3$ conformer equilibrium is observed along the trajectories. The equilibrium populations (p_{3T4}, p_{4T3}) estimated by integrating the g_ω profiles are summarized in Table 1.

Table 1 Average hcc values from the solvated DMPO–OH MD trajectories (labeled T1–T8)

Trajectory	p_{3T4}	$\bar{a}_{H_\beta}$	$\bar{a}_N$
	0	20.1 [18.6] *3.7*	14.4 [15.1] *2.9*
T1	0.5	20.6 [19.0] *3.9*	14.6 [15.2] *2.9*
T2	1.4	19.9 [18.4] *3.6*	14.4 [15.0] *3.0*
T3	7.8	18.9 [17.5] *3.5*	14.2 [14.9] *2.8*
T4	34.1	15.5 [14.2] *2.6*	13.9 [14.5] *2.8*
T5	40.2	14.8 [13.6] *2.5*	14.0 [14.6] *2.8*
T6	71.5	11.4 [10.5] *1.9*	13.6 [14.2] *2.7*
T7	89.7	9.4 [8.6] *1.7*	13.6 [14.2] *2.8*
T8	96.7	8.0 [7.3] *1.3*	13.6 [14.1] *2.8*
	100	7.8 [7.1] *1.2*	13.4 [14.0] *2.8*

p_{3T4}: $^3T_4$-like conformer population values in percent along each trajectory. All $\bar{a}_X$ hcc values are in Gauss, as estimated from PBE0/6-31+G(d) computations (in squarebrackets, CCSD/EPR-II extrapolated values and, in italic, the $\delta^S(\bar{a}_X)$ solvent contribution). For $p_{3T4} = 0/100$ %: extrapolated hcc values based on linear regressions of the trajectory averages

To further analyze the structure of DMPO–OH in solution, we also compute the $g_{2D}(\theta,\phi)$ 2D distribution functions. For the T1 trajectory ($p_{3T4} \approx 1$ %), $g_{2D}(\theta,\phi)$ is centered around (165°, 85°), whereas it is centered around (175°, 45°) for T8 ($p_{3T4} = 97$ %). Hence, H_β is almost axial along T1, while it is equatorial along T8. For the remaining trajectories, $g_{2D}(\theta,\phi)$ appears to be the average of T1 and T8, weighted by the p_{3T4} and p_{4T3} values. Concerning ∠ONCC, its distribution functions correspond to Gaussian profiles centered around 170–175°, with almost negligible contributions for $\theta < 150°$ and $\theta > 210°$, similar to the case of the PROXYL and DMPO–OOH nitroxides we recently investigated [2, 8].

Lastly, the number of solvated DMPO–OH structures involving an intramolecular COH···ON HB is estimated from the distribution functions corrresponding to the $R_{H\cdots O}$ distance between the hydroxyl hydrogen atom and the nitroxide oxygen one (along our trajectories, these functions are all characterized by a sharp peak around 3.8–3.9 Å). Assuming that a HB exists for $R_{H\cdots O} < 2.5$ Å, the integration of these distribution functions exhibits that such an intramolecular HB is observed at most in 0.3 % of the structures for each trajectory.

In conclusion, the DMPO–OH structure in an aqueous medium involves a fast interconversion process between

two major conformations of the five-membered ring ($^3T_4$ and $^4T_3$), and do not present any intramolecular COH$\cdots$ON HB.

3.2 DMPO–OH hcc's in solution

Table 1 shows the $\bar{a}_N$ and $\bar{a}_{H_\beta}$ hcc average values obtained from our QM/MM//MD protocol. Together with $\bar{a}_{H_\gamma}$ values corresponding to the γ^1-hydrogen, they are plotted as a function of p_{3T4} in Fig. 2. The root mean square deviations corresponding to $\bar{a}_N$ and $\bar{a}_{H_\beta}$ are between 5 and 6 Gauss. Since the 2000 nitroxide/water extracted structures are temporally uncorrelated, the uncertainty affecting the average hcc's is about 0.2 Gauss. The γ^2-hydrogen hcc values are always $\pm$0.1 Gauss and are not further discussed.

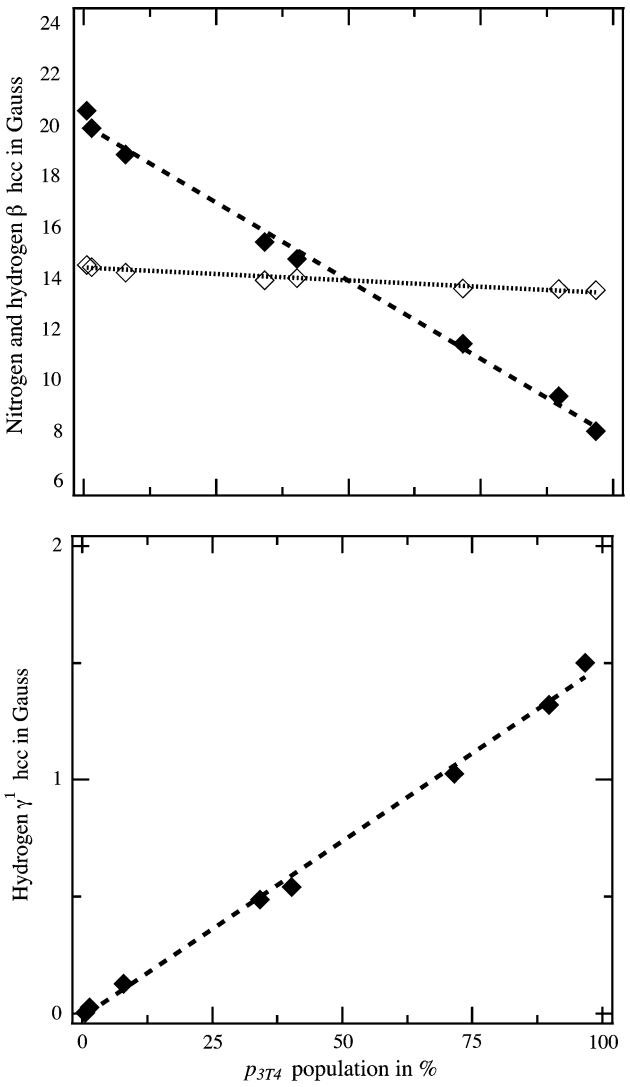

Fig. 2 Hcc values versus p_{3T4} population. *Up* nitrogen (*empty diamonds*) and β-hydrogen (*plain diamonds*) hcc's; *down* γ^1-hydrogen hcc's. *Lines* linear regression fits

Nitrogen, and β- and γ^1-hydrogen hcc values depend linearly on p_{3T4}: the corresponding correlation coefficients are all greater than 0.96. Hence, the magnitude of the DMPO–OH spin densities in aqueous solution is intimately related to the properties of the $^3T_4/^4T_3$ equilibrium. The strongest dependence on this ratio concerns $\bar{a}_{H_\beta}$, whereas a much weaker dependence is observed for $\bar{a}_N$ and $\bar{a}_{H_\gamma}$ (variation of 12 Gauss for $\bar{a}_{H_\beta}$ and of 1 Gauss for $\bar{a}_N$ and $\bar{a}_{H_\gamma}$, as p_{3T4} increases from 0 to 100 %).

We estimate classically the solvent influence on the hcc's by computing the solvent contribution $\delta^S(\bar{a}_X) = \bar{a}_X - \bar{a}^n_X$, where $\bar{a}^n_X$ is the hcc mean value derived from the above-mentioned statistical ensembles, from which the water molecules are discarded. For the nitrogen and oxygen nuclei, $\delta^S(\bar{a}_X)$ is positive (between 1 and 4 Gauss): the solvent is thus responsible for an increase of the corresponding hcc's. On the contrary, the solvent contribution for $\bar{a}_{H_\gamma}$ is negligible (between $-$0.1 and 0.2 Gauss).

The reliability of our PBE0 hcc computations is checked by evaluating the $\delta a_X^{quantum}$ quantum uncertainty as in our previous works [2, 8]. Based on the (θ, ϕ) hcc contours in gas phase corresponding to the MENO–OH model radical and on the (θ, ϕ) 2D distributions computed from the solvated trajectories, we interpolate both the CCSD/EPR-II and PBE0/6-31+G(d) hcc's in gas phase using a bicubic interpolation scheme. The difference between the latter two hcc sets provides $\delta a_X^{quantum}$, which allow us to extrapolate the expected CCSD/EPR-II hcc's of DMPO–OH in solution (Cf. Table 1). Compared to PBE0 values, the CCSD ones are larger (N) and weaker (H_β) by about 1 Gauss. However, the linear dependence of extrapolated CCSD hcc's on p_{3T4}, and thus on the $^3T_4/^4T_3$ equilibrium ratio, is preserved.

Figure 2 shows that a $^3T_4/^4T_3$ equilibrium ratio close to 40/60 % leads to nitrogen and β-hydrogen hcc values in good agreement with the experimental data. In that case, a_N and a_{H_β} are close, about 14–15 Gauss, and the γ^1-hydrogen hcc is weak, smaller than 0.6 Gauss (experimentally, both a_N and a_{H_β} are around 15 Gauss, and no a_{H_γ} splitting is reported [11]). Concerning the energetic results (Cf. Supporting Information), the best agreement between force field and quantum predictions concerning both $^3T_4$-like and $^4T_3$-like conformers of DMPO–OH in gas phase is observed for the T4 force field parameter set, which leads to a $^3T_4/^4T_3$ equilibrium ratio in solution of 34/66 %. This therefore demonstrates the strong internal consistency of our QM/MM//MD combined approach.

4 Conclusion

The present results are in line with those we reported previously for DMPO–OOH, except for the magnitude of

the β-hydrogen hcc, which appears to be 3 to 4 Gauss larger for DMPO–OH than for the two DMPO–OOH conformer families, and whatever the p_{3T4} value (see results of Ref. [8]). We may also note that, whatever p_{3T4}, the γ^1-hydrogen hcc is twice smaller in the case of DMPO–OH than for DMPO–OOH (respectively, 0.6 and 1.2 Gauss for a 1:1 $^3T_4/^4T_3$ ratio, for instance). While γ-hydrogen atoms are responsible for an alternate linewidth in DMPO–OOH EPR spectrum, they are completely silent in the DMPO–OH one.

In agreement with the well-established experimental interpretation, and with our previous theoretical results concerning DMPO–OOH, our computations clearly show that there is no unique (i.e., long-lived) DMPO–OH structure in aqueous solution from which the spectromagnetic properties originate. We should rather consider an equilibrium between $^3T_4$-like and $^4T_3$-like conformations of the DMPO–OH five-membered ring. Accordingly, the apparent hcc's of DMPO–OH obtained from its EPR spectrum can be interpreted as the 1:1 averages of the hcc's of the pure $^3T_4$ and $^4T_3$ conformers (in a fast exchange process).

This work establishes firmly the reliability of the simulation protocol we set up to get quantitative estimates of flexible nitroxide hcc's in an aqueous medium. It represents thus an accurate and robust theoretical approach, which can be used at the earlier stage of development of new challenging spin traps to study their corresponding nitroxide spin adducts.

Acknowledgments All of the computations were performed on the large-scale facilities of the "Centre de Calcul et de Recherche Technologique" (CCRT) of the French Nuclear Agency (CEA) and of the "Centre Informatique National de l'Enseignement Supérieur" (CINES), and at the "Centre Régional de Compétences en Modélisation Moléculaire" (CRCMM) in Marseille. This work was granted access to the HPC resources of CCRT and CINES under the allocation 2010082226 made by GENCI (Grand Équipement National de Calcul Intensif).

References

1. Houriez C, Ferré N, Masella M, Siri D (2008) J Chem Phys 128:244504
2. Houriez C, Ferré N, Siri D, Masella M (2009) J Phys Chem B 113:15047
3. Stendardo E, Pedone A, Cimino P, Menziani MC, Crescenzi O, Barone V (2010) Phys Chem Chem Phys 12:11697–11709
4. Pavone M, Benzi C, De Angelis F, Barone V (2004) Chem Phys Lett 395:120
5. Pavone M, Cimino P, De Angelis F, Barone V (2006) J Am Chem Soc 128:4338
6. Asher JR, Kaupp M (2008) Theor Chem Acc 119:477
7. Rinkevicius Z, Frecus B, Murugan NA, Vahtras O, Kongsted J, Ågren H (2012) J Chem Theory Comput 8:257–263
8. Houriez C, Ferré N, Siri D, Tordo P, Masella M (2010) J Phys Chem B 114:11793–11803
9. Harbour J, Chow V, Bolton J (1974) Can J Chem 52:3549
10. Clément J-L, Ferré N, Siri D, Karoui H, Rockenbauer A, Tordo P (2005) J Org Chem 70:1198
11. Lloyd RV, Hanna PM, Mason RP (1997) Free Radic Biol Med 22:885–888
12. Villamena FA, Hadad CM, Zweier JL (2003) J Phys Chem A 107:4407–4414
13. Villamena FA, Hadad CM, Zweier JL (2004) J Am Chem Soc 126:1816–1829
14. Rosen G, Beselman A, Tsai P, Pou S, Mailer C, Ichikawa K, Robinson B, Nielen R, Halpern H, MacKerell A (2004) J Org Chem 69:1321–1330
15. Villamena FA, Merle JK, Hadad CM, Zweier JL (2005) J Phys Chem A 112:6089–6098
16. Masella M, Cuniasse P (2003) J Chem Phys 119:1866
17. Houriez C, Ferré N, Masella M, Siri D (2009) J Mol Struct (Theochem) 898:49
18. Cremer D, Pople J (1975) J Am Chem Soc 97:1358
19. Kaupp, M, Buehl, M, Malkin, VG (eds) (2004) Calculation of NMR and EPR parameters. Wiley-VCH, Weinheim
20. Frisch MJ et al (2004) Gaussian 03, revision C.02. Gaussian, Inc., Wallingford
21. Ferré N, Ángyán JG (2002) Chem Phys Lett 356:331